Electronic Supplementary Information

Hollow Cubic CdS@CoS/WS_2 Dual S-Scheme Heterojunction Superstructure Towards Optimized Photothermal-Photocatalytic Performance

Weifeng Kong[a], Zipeng Xing[a,*], Hang Zhang[a, c], Bin Fang[a], Yongqian Cui[a], Zhenzi Li[b], Peng Chen[a,*], Wei Zhou[a, b*]

[a] Department of Environmental Science, School of Chemistry and Materials Science, Key Laboratory of Functional Inorganic Material Chemistry, Ministry of Education of the People's Republic of China, Heilongjiang University, Harbin 150080, P. R. China. Email: xingzipeng@hlju.edu.cn; jehugu@gmail.com; zwchem@hotmail.com

[b] Shandong Provincial Key Laboratory of Molecular Engineering, School of Chemistry and Chemical Engineering, Qilu University of Technology (Shandong Academy of Sciences), Jinan 250353, P. R. China

[c] Heihe Ecological Environment Information and Emergency Support Center, Heihe 161404, P. R. China

Experimental section

1. Characterization

The morphology characteristics of the sample was observed using a scanning electron microscope (SEM, JSM 6700F, JEOL). Transmission electron microscopy (TEM) images were taken on a JEM-2100 field emission electron microscope at an accelerating voltage of 200 kV. The crystallinity of the CdS@CoS/WS_2 was characterized by X-ray diffraction (XRD) with a Bruker D8 advance under Cu Kα radiation (λ = 1.5406 Å). X-ray photoelectron spectroscopy (XPS) was recorded on a PerkinElmer RBD upgraded PHI-5000C ESCA system. UV-vis diffuse reflection spectra (DRS) were recorded on a UV-vis spectrophotometer (UV-2550, Shimadzu) with an integrating sphere attachment, and $BaSO_4$ was used as the reference material. The steady-state photoluminescence (PL) spectra were measured with a PE LS 55 spectrofluoro-photometer at excitation wavelength of 325 nm. Transient-state photoluminescence (TS-PL) spectra were recorded with a single photon counting spectrometer from (Edinburgh Instrument, FLS 920). The work function of samples was tested by Scanning Kelvin probe (SKP) (SKP5050 system, Scotland). The work function of samples was tested by Scanning Kelvin probe (SKP) (SKP5050 system, Scotland). The electron spin resonance (ESR) spectra under visible light irradiation were tested with ESR spectrometer (Bruker model A300). The temperature of the sample was measured using the Testo 865 infrared thermograph.

2. Photocatalytic hydrogen evolution

The photocatalytic H_2 evolution experiments were conducted in an online hydrogen generation system. During the photocatalytic hydrogen evolution reaction, the samples (100 mg) were dispersed in 100 mL of methanol/H_2O solution ($V_{methaol}$: V_{H_2O} = 1:4). Before light irradiation, the reactor and the entire gas circulating system were fully degassed to remove air using a vacuum pump for 30 min. Before the photocatalytic reactions, the dispersion was sonicated for 10 min. A 300 W Xe lamp was used as the light source that simulated the full-spectrum source. The Xe lamp coupled with a UV cut-off filter (> 420 nm) was used to obtain the visible light. The NIR light was implemented by using the Xe lamp, coupled with a UV–vis cut-off filter (> 800 nm). The photocatalytic H_2 evolution was analyzed using a gas chromatograph (SP7800, TCD, molecular sieves 5 Å, N_2 carrier, Beijing Keruida Limited).

3. Photocatalytic degradation

Photocatalytic experiments were carried out by adding 50 mg of photocatalyst to 100 mL of solution containing Tetracycline (TC) (10 mg/L) or Bisphenol A (BPA) (10 mg/L). Before the photocatalytic experiments, the solution containing the pollutants and the photocatalyst was placed in a dark room for 30 min to get the adsorption–desorption equilibrium. Then, the solution was irradiated under a 300 W Xenon lamp. Every 15 min, 3 mL of each liquid sample was removed from the beaker and filtered with 0.22 μm Millipore filter heads for subsequent concentration tests. The kinetic concentrations of these contaminants at pre-determined time intervals were analyzed by T6 UV-vis spectrophotometer. The photocatalytic degradation efficiency was calculated from the following equation:

$$\eta = \left(\frac{(C_0 - C)}{C_0}\right) * 100\% \quad (1)$$

where η is the photocatalytic degradation efficiency, C_0 is the initial concentration of the contaminants, and C is the concentration of the contaminants at reaction time t. During the test, room temperature was kept at 20 ± 2 °C.

4. Photoelectrochemical tests

The electrochemical measurement was carried out by a standard three-electrode system. 50 mg as-prepared sample was dispersed in 35 mL ethanol and then spread uniformly on indium-tin oxide (ITO) conductor glass as work electrode, while Ag/AgCl as reference electrode, Pt foil as counter electrode and 1.0 M Na_2SO_4 aqueous solution as electrolyte. The transient photocurrent of the sample was obtained by multiple on/off visible light irradiation, with a period of 20 s. Electro-chemical impedance spectroscopy was measured with amplitude of 5 mV and frequencies varying from 0.01 to 10000 Hz.

5. Photothermal test

The photothermal tests of as-prepared samples were performed as follows. Amounts of 0.1 g of samples were loaded on a white paper, and the initial temperature was controlled at room temperature. The temperature of the sample was measured using a Testo 865 infrared thermograph. A 300 W Xenon lamp with a 420 nm cut-off filter was used as a light source to treat CdS, CdS@CoS, CdS/WS_2 and CdS@CoS/WS_2.

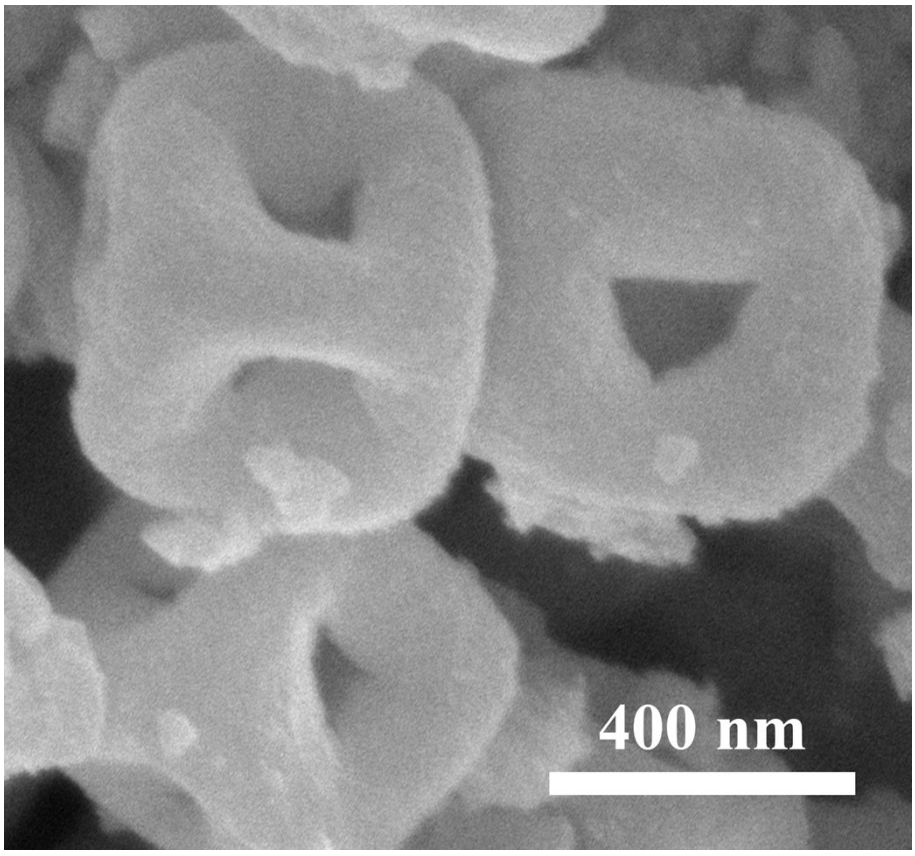

Fig. S1. SEM image of CdS.

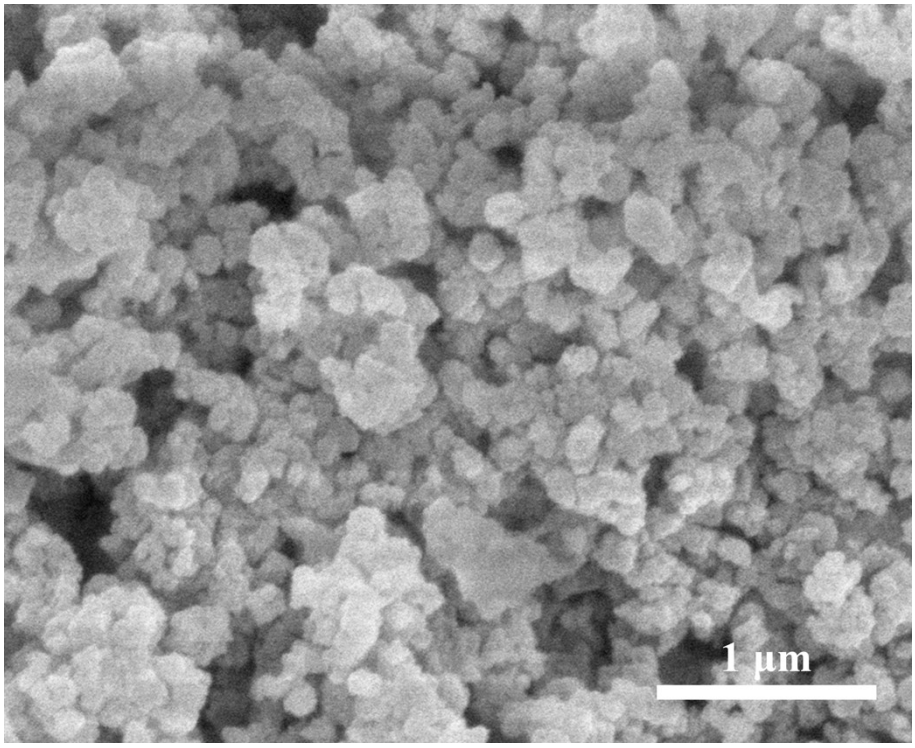

Fig. S2. SEM image of CoS.

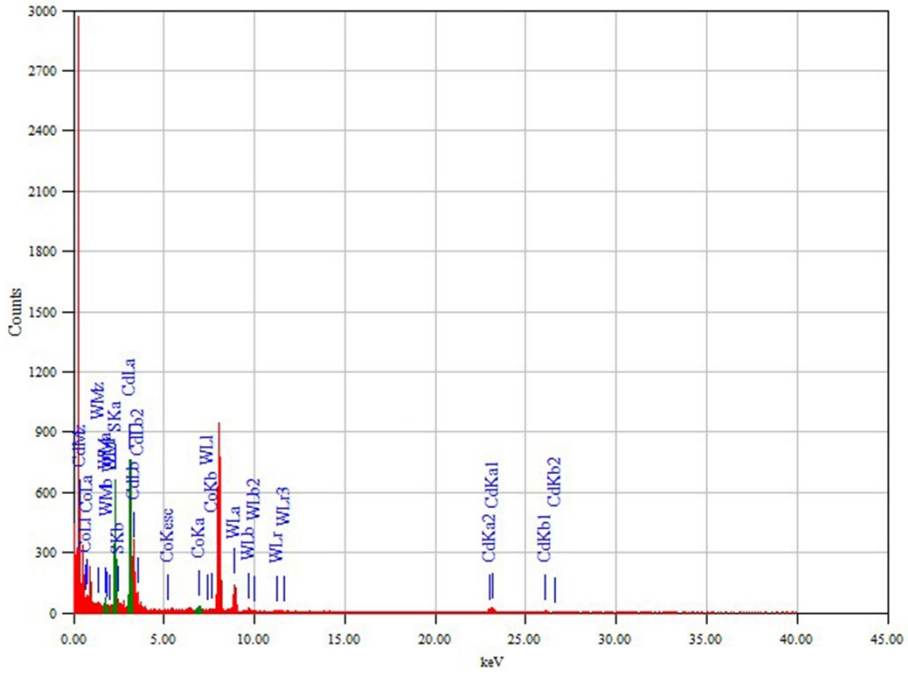

Fig. S3. The corresponding TEM-EDX spectrum of Cd, Co, S and W elements of CdS@CoS/WS_2.

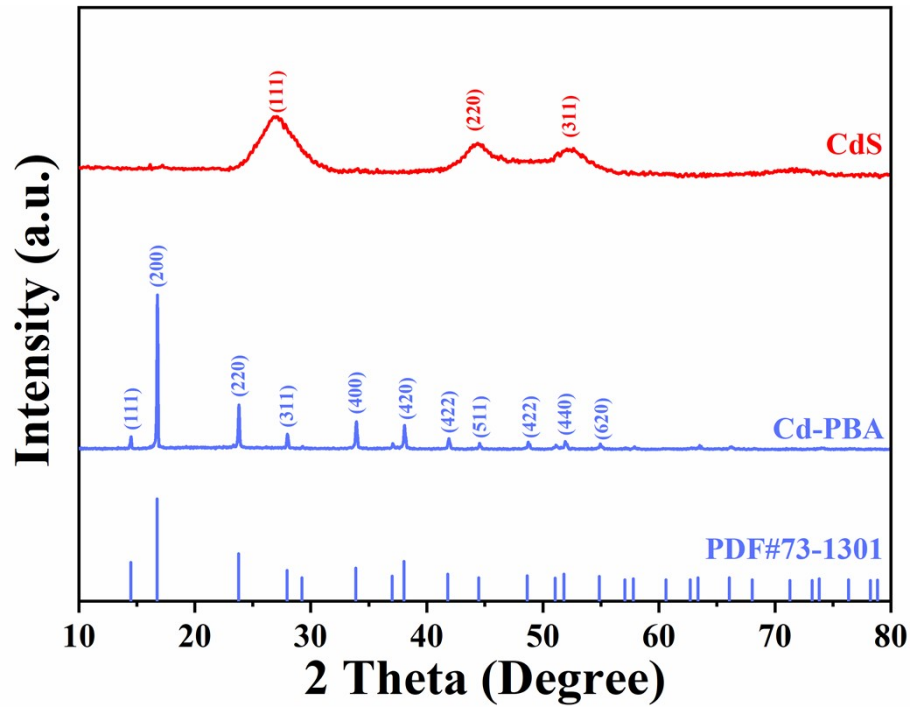

Fig. S4. Typical XRD patterns of Cd-PBA and CdS.

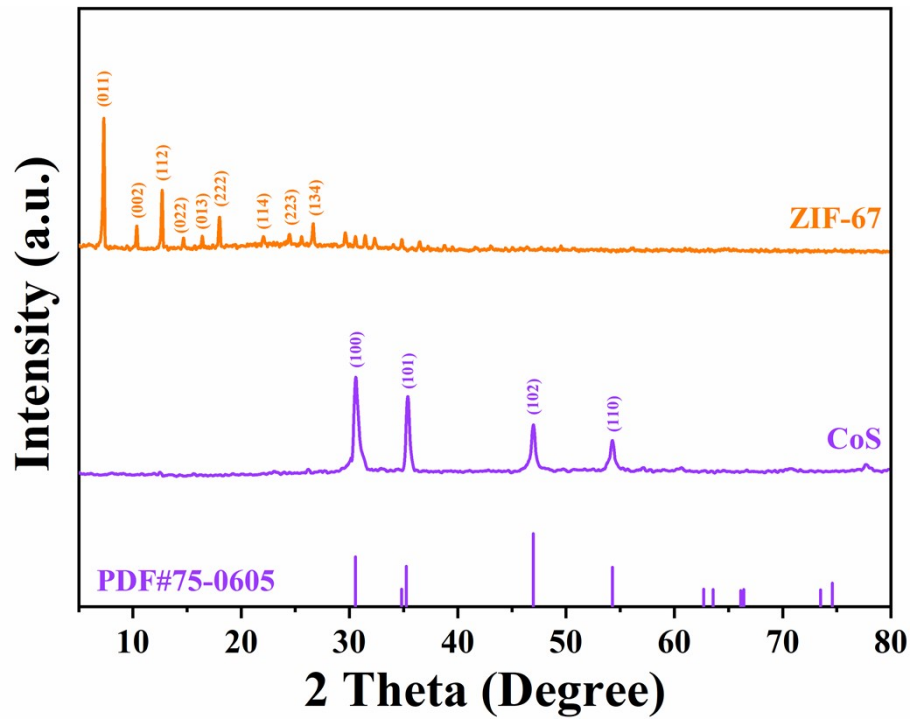

Fig. S5. Typical XRD patterns of ZIF-67 and CoS.

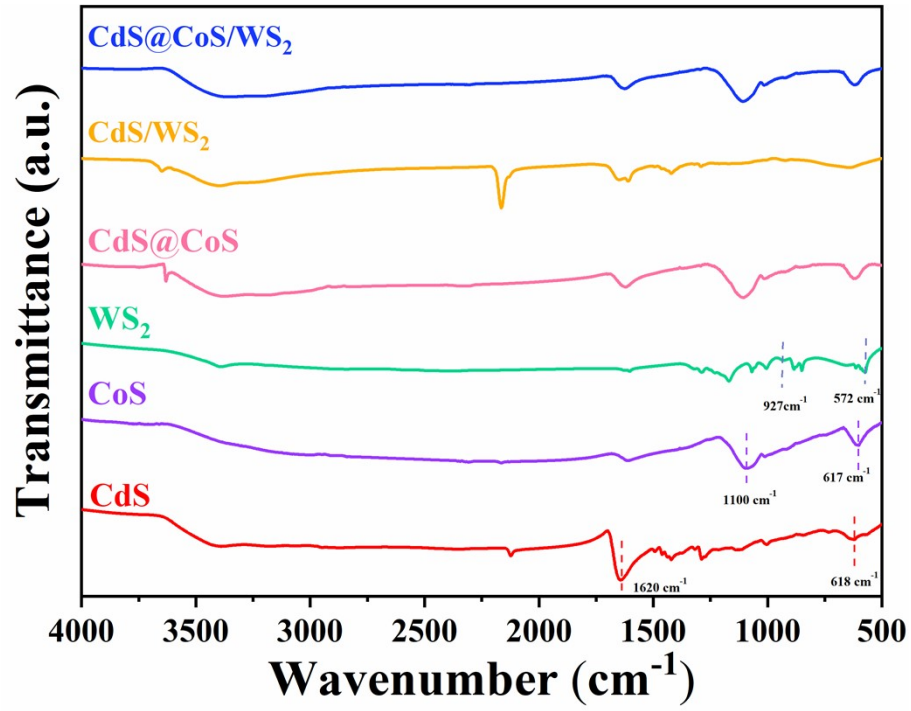

Fig. S6. FT-IR spectra of CdS, CoS, WS_2, CdS@CoS, CdS/WS_2 and CdS@CoS/WS_2.

Fig. S7. Digital photographs of CdS, CoS, WS_2, CdS/WS_2, CdS@CoS and CdS@CoS/WS_2.

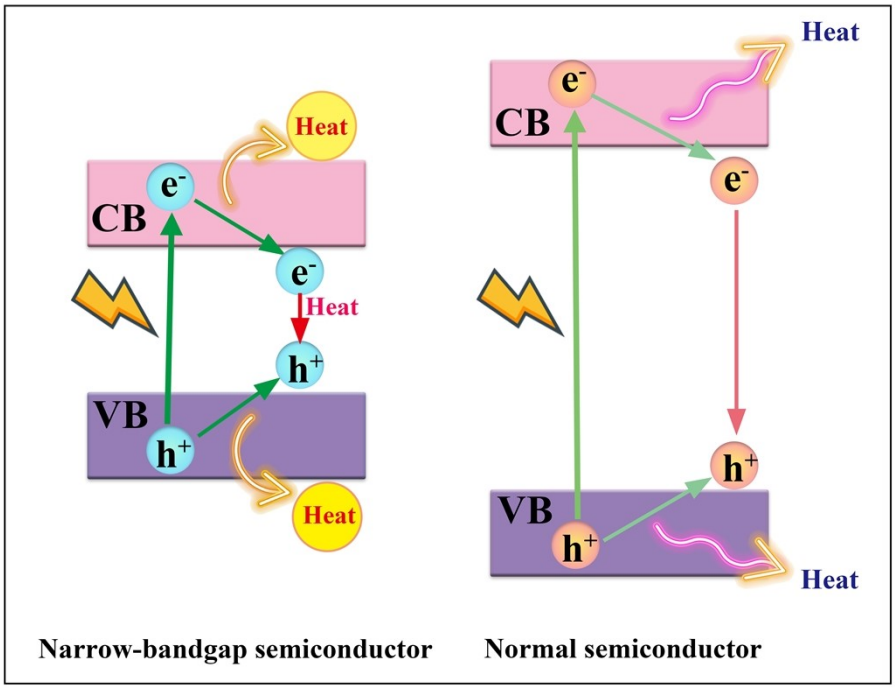

Fig. S8. Photothermal schematics of two different types of semiconductors.

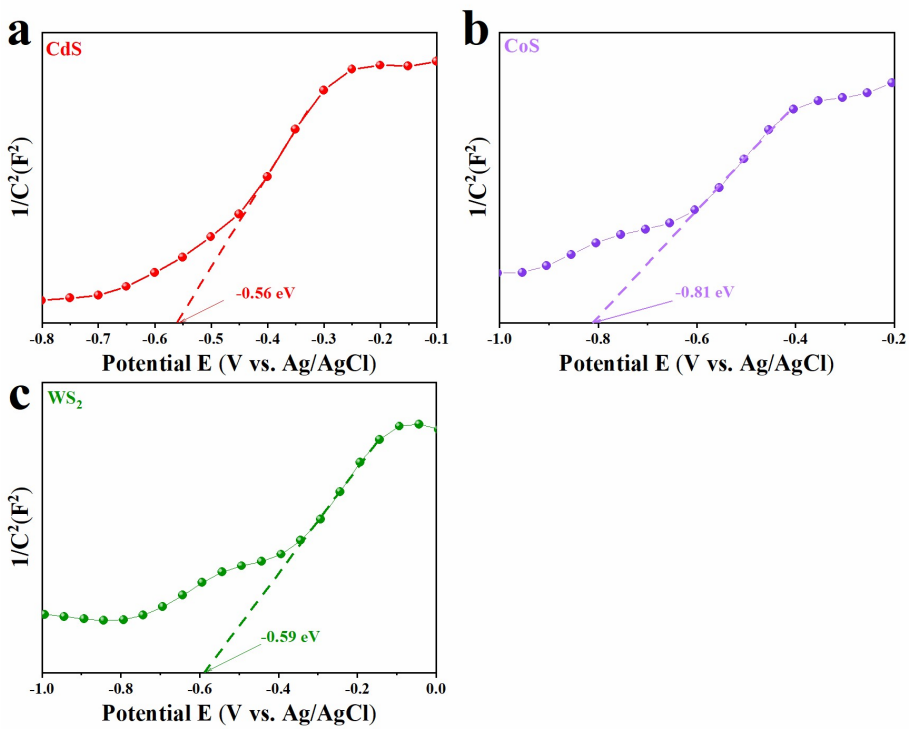

Fig. S9. Mott-Schottky plots of CdS (a), CoS (b) and WS_2 (c), respectively.

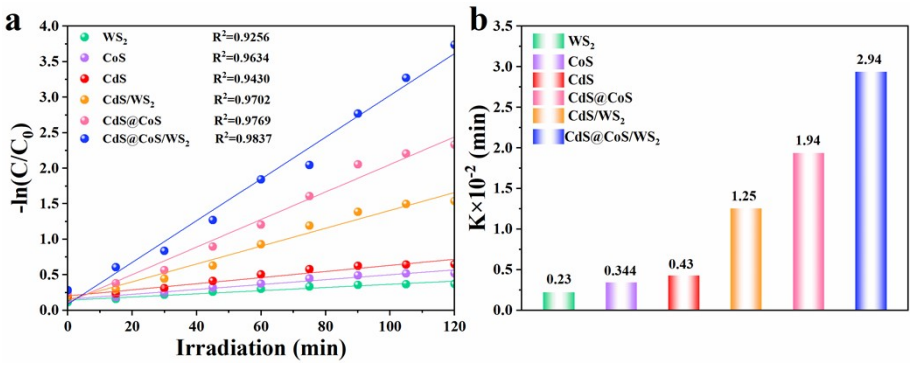

Fig. S10. Relevant pseudo first-order kinetics fitting curves (a) and apparent rate constants (b) of photocatalytic TC reduction with different samples.

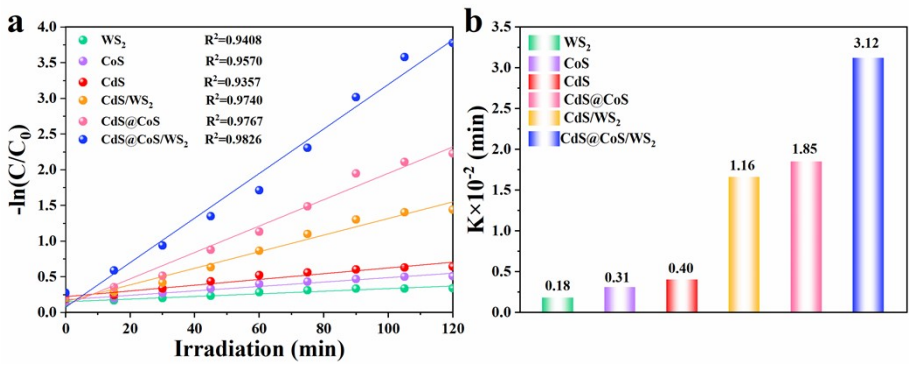

Fig. S11. Relevant pseudo first-order kinetics fitting curves (a) and apparent rate constants (b) of photocatalytic BPA reduction with different samples.

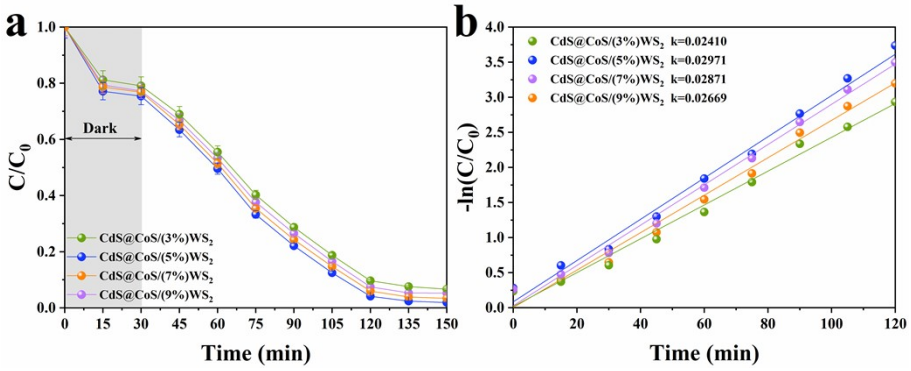

Fig. S12. Correlation pseudo-first-order kinetic fitting curves (a) and apparent rate constants (b) for the photocatalytic degradation of TC by CdS@CoS/(3%)WS_2, CdS@CoS/(5%)WS_2, CdS@CoS/(7%)WS_2 and CdS@CoS/(9%)WS_2.

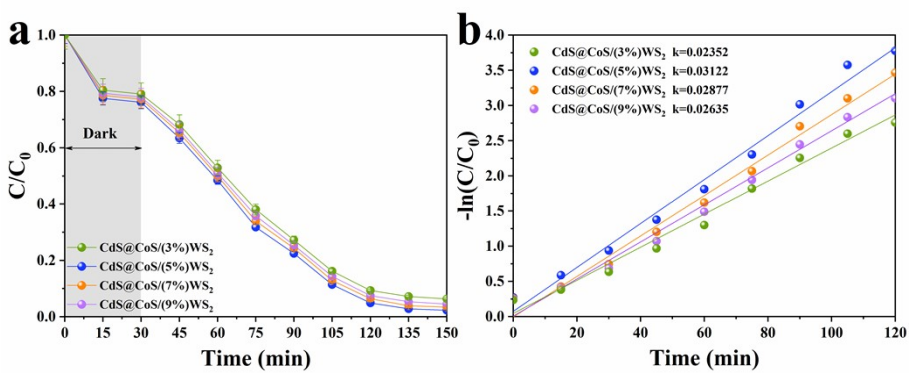

Fig. S13. Correlation pseudo-first-order kinetic fitting curves (a) and apparent rate constants (b) for the photocatalytic degradation of BPA by CdS@CoS/(3%)WS_2, CdS@CoS/(5%)WS_2, CdS@CoS/(7%)WS_2 and CdS@CoS/(9%)WS_2.

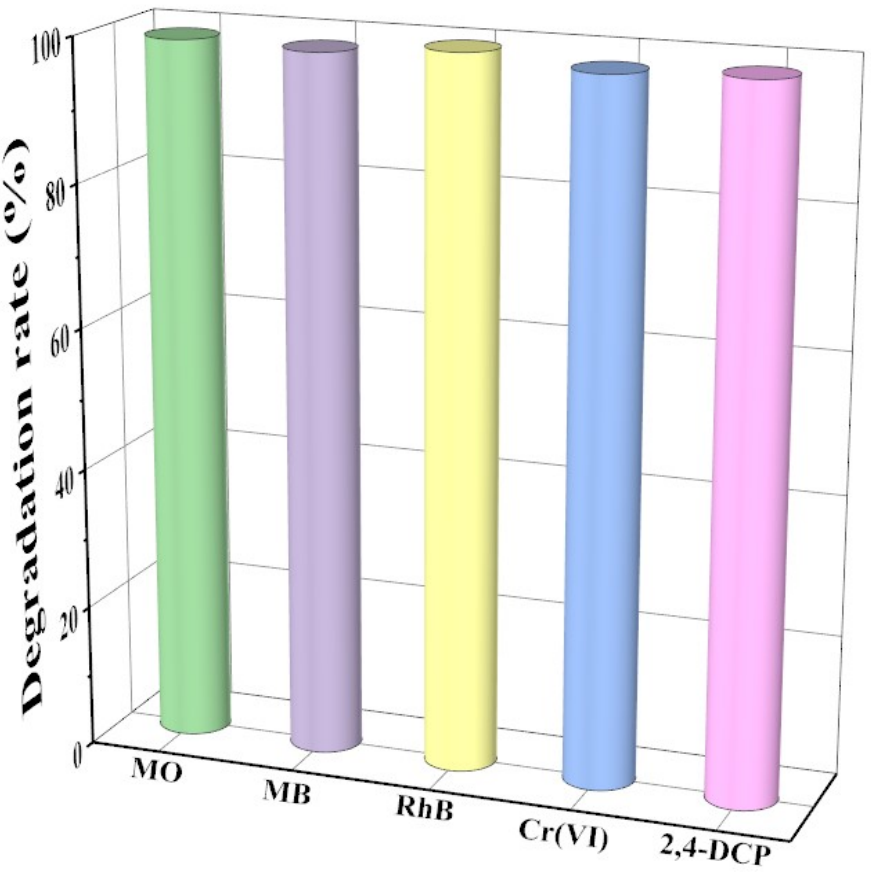

Fig. S14. Photocatalytic degradation rates of CdS@CoS/WS_2 for different pollutants within 150 min degradation process.

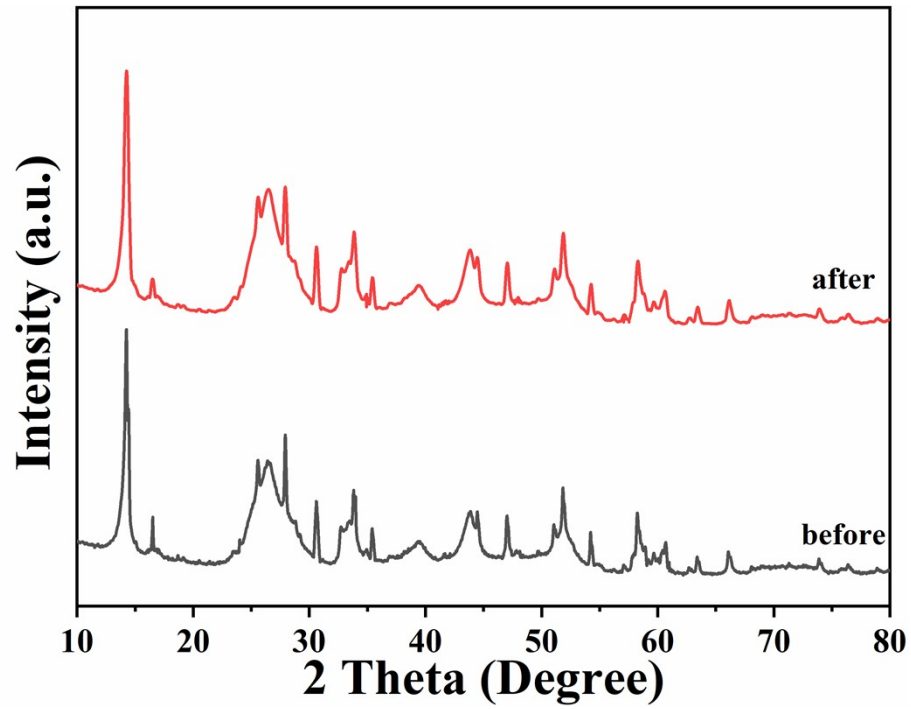

Fig. S15. XRD patterns of CdS@CoS/WS_2 sample before and after photocatalytic reaction.

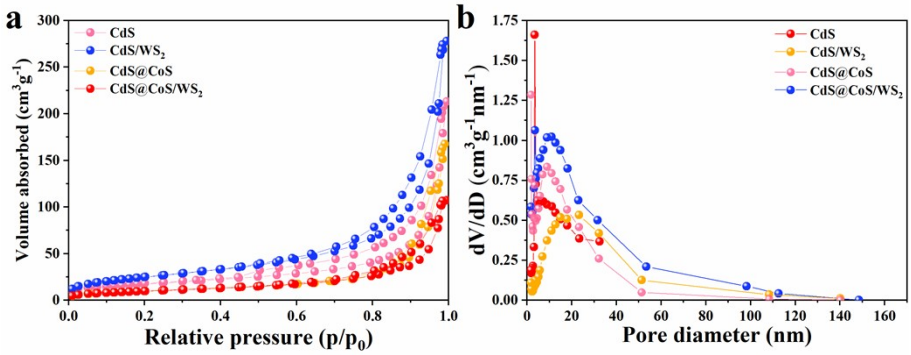

Fig. S16. N_2 adsorption-desorption isotherms (a) and the corresponding pore size distributions (b) of CdS, CdS@CoS, CdS/WS_2 and CdS@CoS/WS_2.

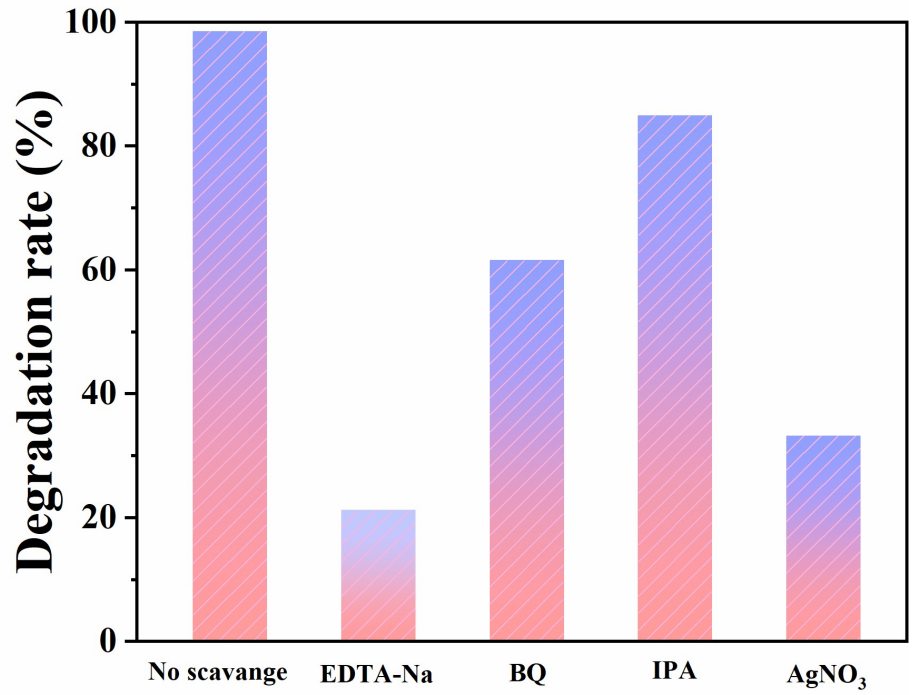

Fig. S17. The radical species trapping experiments for photocatalytic degradation of MB over CdS@CoS/WS_2 photocatalyst under visible light irradiation.

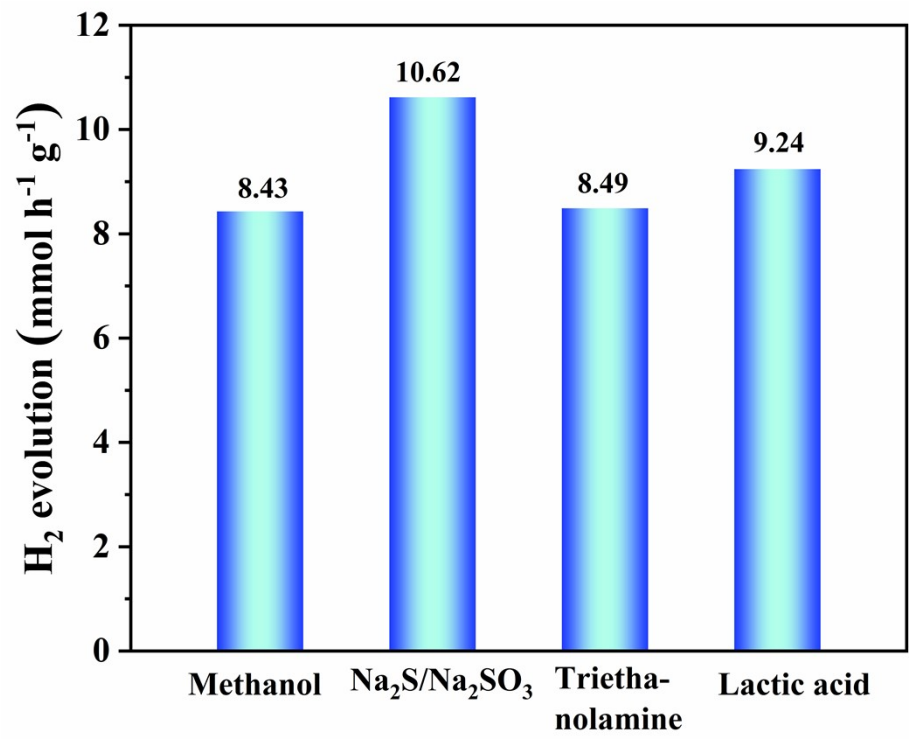

Fig. S18. Photocatalytic H_2 evolution rates of CdS@CoS/WS_2 in different sacrificial agents.

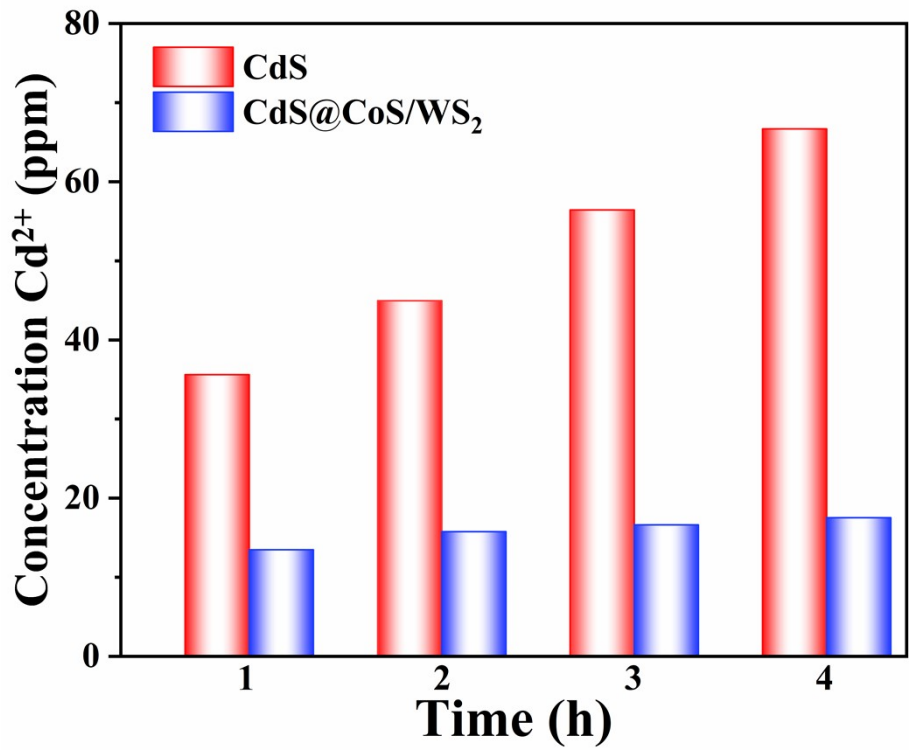

Fig. S19. ICP-OES results of CdS and CdS@CoS/WS_2 photocatalysts.

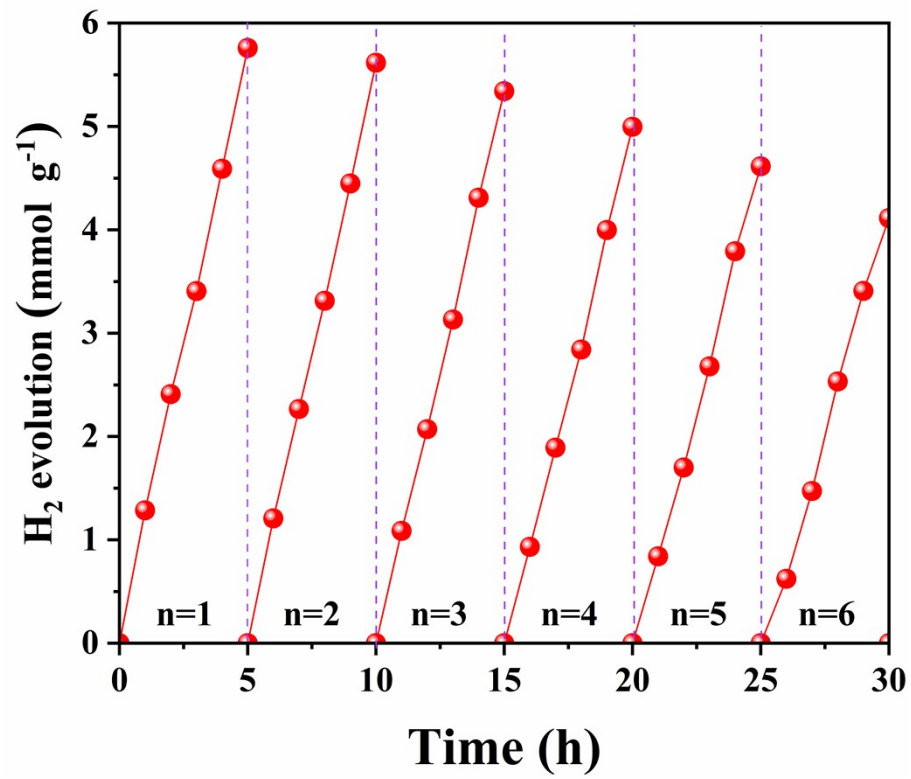

Fig. S20. Cycle stability test of photocatalytic H_2 evolution for CdS.

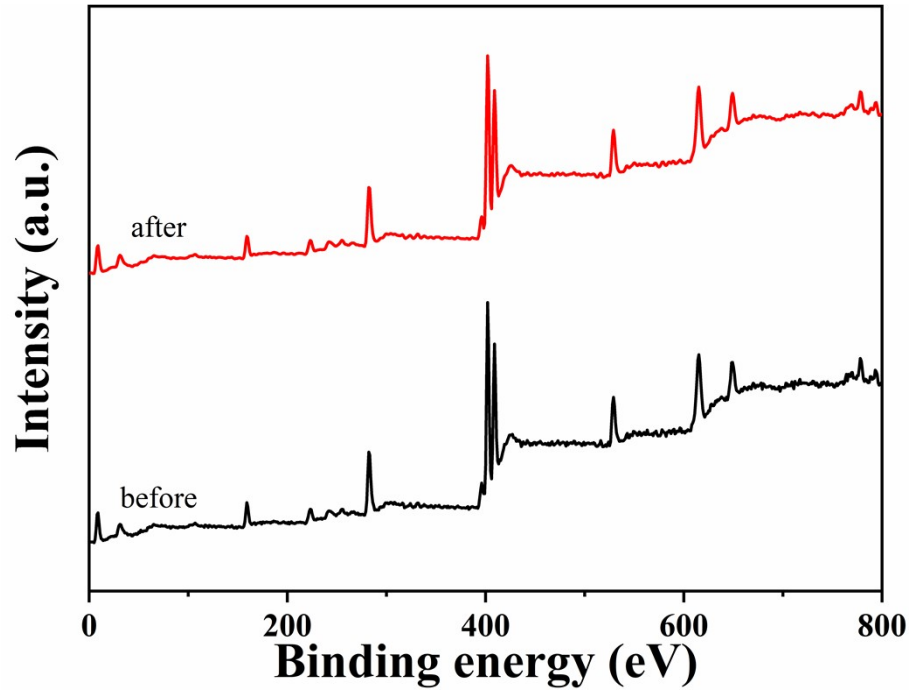

Fig. S21. XPS patterns of CdS@CoS/WS_2 sample before and after photocatalytic reaction.

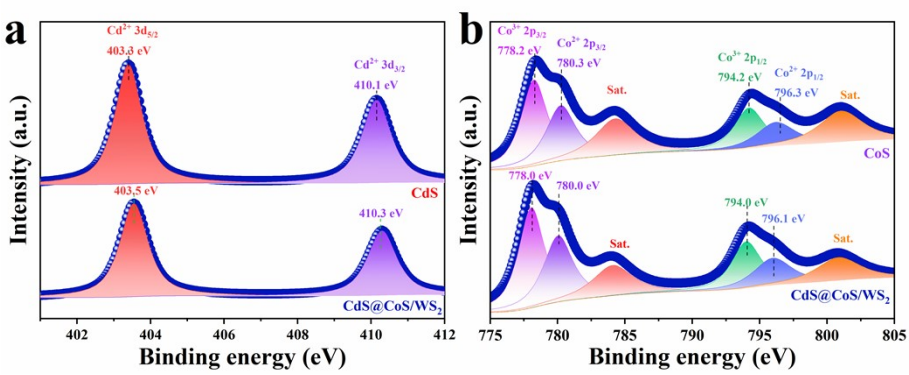

Fig. S22. The in-situ XPS spectra of Cd 3d (a) and Co 2p (b). (Under simulated sunlight irradiation).

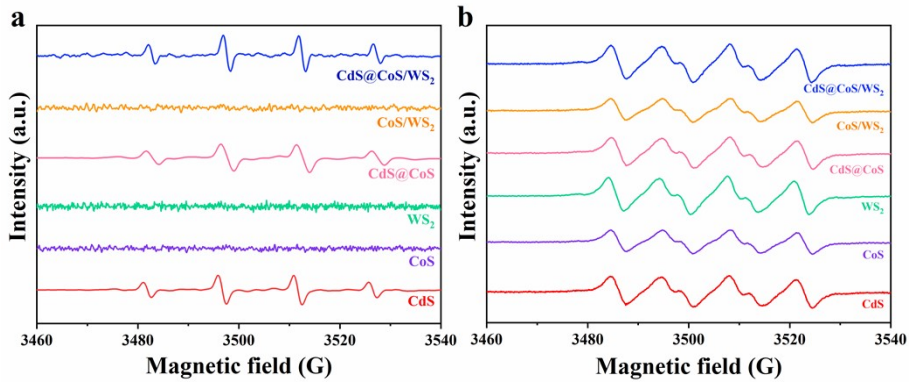

Fig. S23. ESR signals of DMPO-•OH and DMPO-•O_2^- in the presence of CdS, CoS, WS_2, CdS@CoS, CoS/WS_2 and $CdS@CoS/WS_2$ after 3 min irradiation.

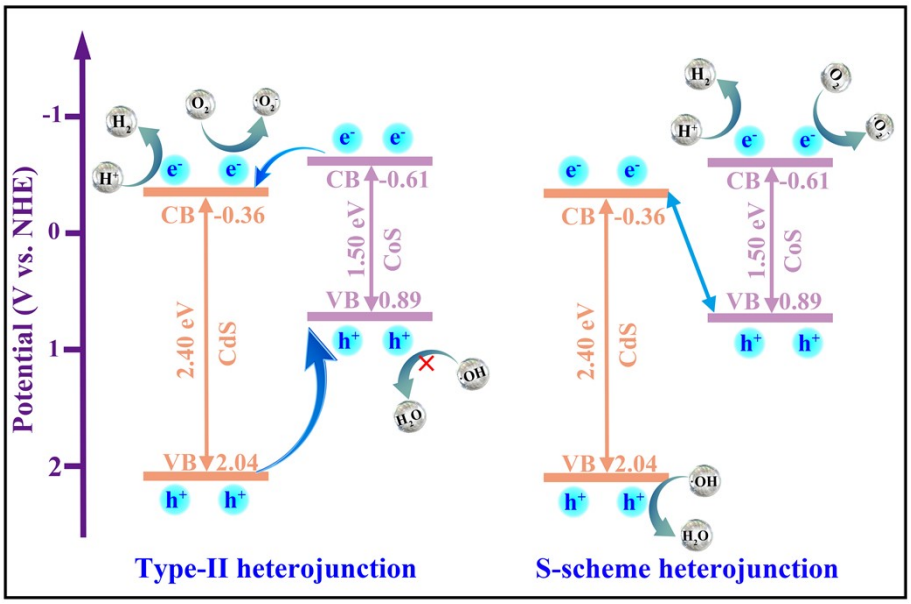

Fig. S24. Schematic diagram of the possible heterojunction mechanism for hollow CdS@CoS heterojunction superstructure.

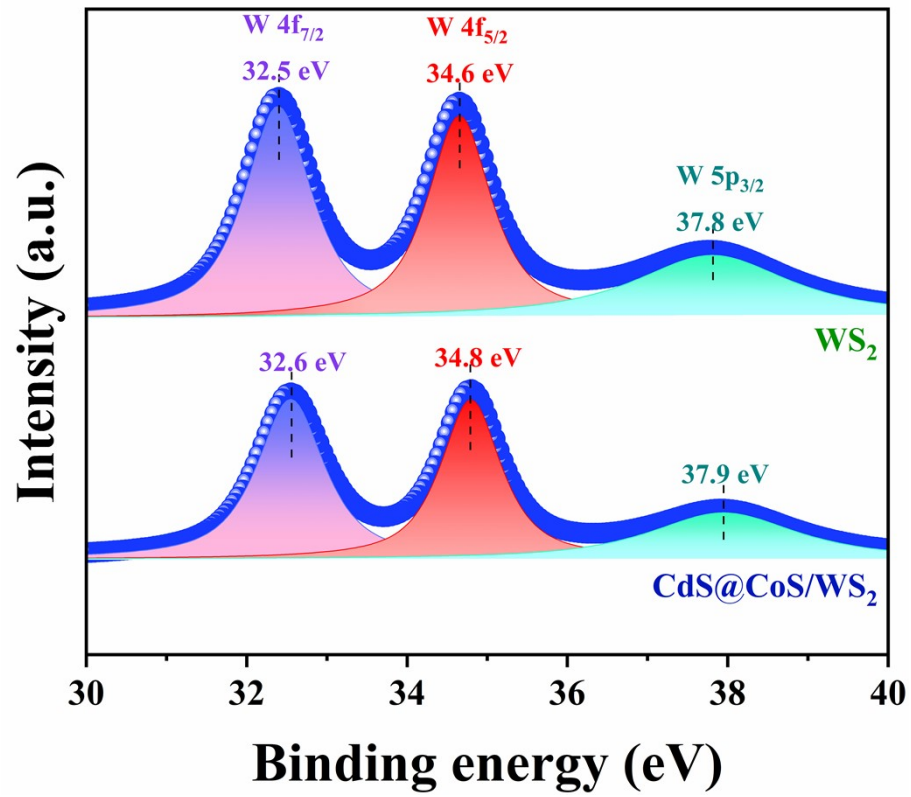

Fig. S25. The in-situ XPS spectra of W 4f for different samples. (Under simulated sunlight irradiation).

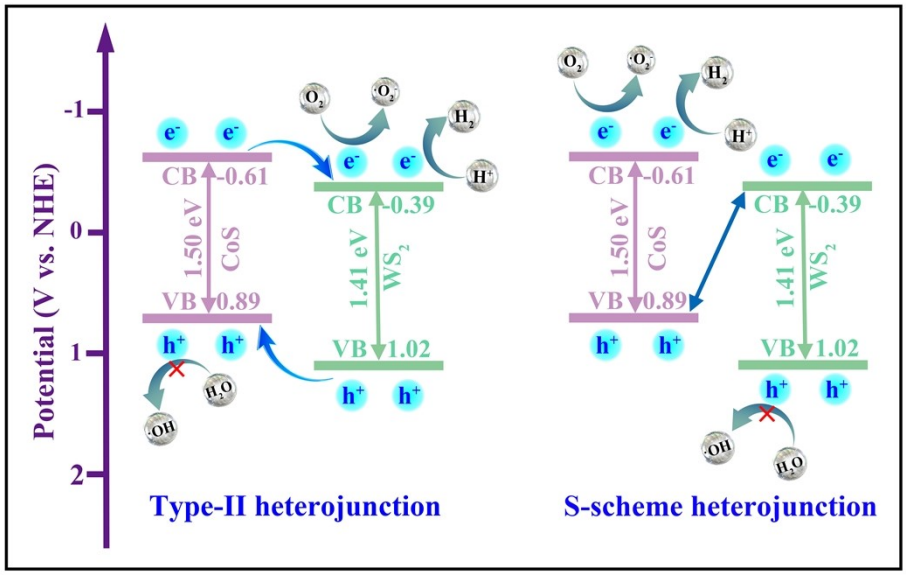

Fig. S26. Schematic diagram of the possible heterojunction mechanism for CoS/WS_2 heterojunction superstructure.

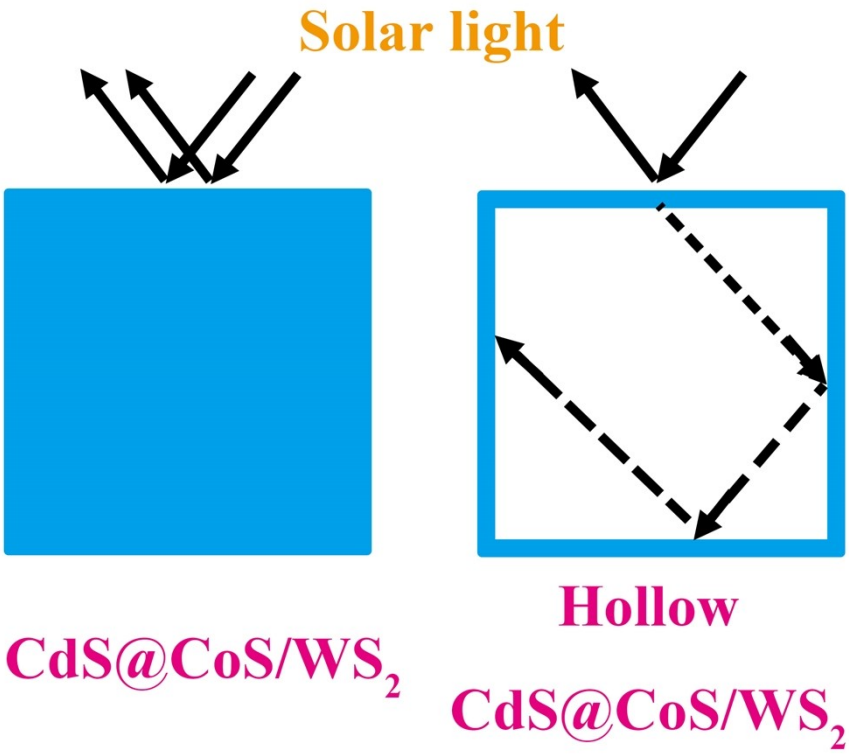

Fig. S27. Schematic diagram of multiple reflections within the CdS@CoS/WS_2 hollow superstructure under solar light irradiation.

Table S1. Results of the exponential decay-fitted parameters for the fluorescence lifetime of as-prepared samples.

Photocatalyst	B_1	τ_1(ns)	B_2	τ_2(ns)	τ(ns)
CdS	6065.887	2.451	157.170	12.271	3.580
CdS/WS_2	7849.813	2.578	202.992	12.272	3.640
CdS@CoS	6825.647	2.645	216.243	12.067	3.834
CdS@CoS/WS_2	9069.851	2.746	247.991	13.273	3.974

Table S2. Performance comparison of different photocatalysts for photocatalytic H_2 evolution

Photocatalyst	Light Source	H_2 evolution rate (mmol h^{-1} g^{-1})	Ref.
CdS@Co_9S_8	Xe lamp (300 W, λ ≥ 420 nm)	0.79	[1]
WS_2-WO_3•H_2O/g-C_3N_4	Xe lamp (300 W, λ ≥ 420 nm)	1.27	[2]
CoP/TiO_2	Xe lamp (300 W)	8.35	[3]
CdS nanosheets	Xe lamp (300 W)	6.890	[4]
$H_{0.53}WO_3$/CdS	Xe lamp (300 W, λ ≥ 420 nm)	2.003	[5]
$Cs_{0.33}WO_3$/CdS	Xe lamp (300 W, λ ≥ 420 nm)	0.06	[6]
CdS@CoS/WS_2	**Xe lamp (300 W, λ ≥ 420 nm)**	**8.43**	**This work**

Table S3. Comparison of pollutants removal for different photocatalysts under light irradiation.

Photocatalysts	Light source	Degradation rate	pollutant	Ref.
CDs-$ZnIn_2S_4$	300W Xe lamp (λ>420nm)	83%	TC	[7]
Co_9S_8@$ZnIn_2S_4$/CdS	300 W Xe lamp (λ≥420 nm)	90.62%	BPA	[8]
CDs@PCN-222@PNIPAM	300 W Xe lamp (λ≥420 nm)	90.93%	TC	[9]
WO_3/$CdWO_4$	500 W Xe lamp	81.6%	TC	[10]
Bi/BOI	350 W Xe lamp (λ≥420 nm)	90%	BPA	[11]
ZnO-CdO-RGO	UV light irradiation (30-watt, 365 nm)	81.69%	BPA	[12]
CdS@CoS/WS_2	**Xe lamp (300 W, λ ≥ 420 nm)**	**98.9%** **99.1**	**TC** **BPA**	**This work**

References

[1] B. Qiu, Q. Zhu, M. Du, L. Fan, M. Xing and J. Zhang, *Angew. Chem., Int. Ed.*, 2017, **56**, 2684-2688.

[2] X. Wang, G. Hai, B. Li, Q. Luan, W. Dong and G. Wang, *Chem. Eng. J.*, 2021, **426**, 130822.

[3] X. Yue, S. Yi, R. Wang, Z. Zhang and S. Qiu, *Small*, 2017, **13**, 1603301.

[4] W. Li, X. Wang, Q. Ma, F. Wang, X. S. Chu, X. C. Wang and C. Y. Wang, *Appl. Catal., B*, 2021, **284**, 119688.

[5] L. Zhang, H. Zhang, B. Wang, X. Huang, F. Gao, Y. Zhao, S. Weng and P. Liu, *J. Mater. Chem. A*, 2019, **7**, 1076-1082.

[6] N. Li, H. Fan, Y. Dai, J. Kong and L. Ge, *Appl. Surf. Sci.*, 2020, **508**, 145200.

[7] C. H. W. Shi, Y. Fu, F. Guo, Y. Tang, X. Yan, *Chem. Eng. J.*, 2022, **433**, 133741.

[8] Y. Zhang, Y. Wu, L. Wan, H. Ding, H. Li, X. Wang and W. Zhang, *Appl. Catal., B*, 2022, 121255.

[9] Z. Xia, B. Shi, W. Zhu and C. Lu, *Chem. Eng. J.*, 2021, **426**, 131794.

[10] F. Rong, Q. Lu, H. Mai, D. Chen and R. A. Caruso, *ACS Appl. Mater. Interfaces.*, 2021, **13**, 21138-21148.

[11] X. Liu, X. Xiong, S. Ding, Q. Jiang and J. Hu, *Catal. Sci. Technol.*, 2017, **7**, 3580-3590.

[12] S. Kumar, R. D. Kaushik and L. P. Purohit, *J. Hazard. Mater.*, 2022, **424**, 127332.